

Steffen Hein

A DSC approach to Computational Fluid Dynamics

Abstract This paper presents the Dual Scattering Channel (DSC) numerical solution of the NAVIER-STOKES equations for viscous quasi-incompressible flow in the OBERBECK-BOUSSINESQ approximation. The implementation in hexahedral non-orthogonal mesh is outlined. A numerical example illustrates the approach.

MSC-classes: 65C20, 65M06, 76D05

Westerham, March 31, 2006

1. Introduction

Dual Scattering Channel (DSC) schemes are characterized by a two-step cycle of iteration which alternately updates the computed fields within cells and on their interfaces. If the updating instructions are explicit, then a near-field interaction principle leads to the typical structure of the DSC algorithm and to a scattering process interpretation. A pair of vectors that represent the same field within a cell and on its surface essentially constitutes a *scattering channel*. Equivalently, scattering channels are sometimes defined as pairs of distributions that 'measure' the field within the cell and on one of its faces. A well known DSC scheme is the Transmission Line Matrix (TLM) numerical method along JOHNS' line [JoB] wherein transmission line links visualise the scattering channels. The TLM picture of wave propagation fails in Computational Fluid Dynamics, thus giving rise to the far more general DSC setup.

In technical depth, DSC schemes and their relation to the TLM method have been analysed in [He1]. Another study shows that they are unconditionally stable under quite general circumstances, made tangible with the notion of α -*passivity* [He2]. DSC schemes are particularly suitable for handling boundary conditions, non-orthogonal mesh, or also for replacing a staggered grid where otherwise need of such is.

In section 2 we first recapitulate some characteristic features of DSC schemes, which in extenso are treated in [He1], before we sketch in section 3 the OBERBECK-BOUSSINESQ approximation to the NAVIER-STOKES equations. The DSC model then outlined in section 4 represents a *prototype*, first

of all. In fact, the BOUSSINESQ equations for viscous quasi-incompressible flow, inspite of retaining the often predominant non-linear advective term of the NAVIER-STOKES momentum equations, can only claim limited range of validity, due to their well known simplifications. The OBERBECK-BOUSSINESQ approach is yet prototypical also in providing a basis for many turbulence models [ATP] which can be implemented following the general guide lines of this paper.

The algorithm with non-orthogonal hexahedral mesh cell outlined in section 4 has only recently been implemented by SPINNER, where it is directly coupled to a Maxwell field solver, allowing thus for computing conductive and convective heat transfer simultaneously with the heat sources of a lossy Maxwell field. Besides the underlying ideas and simplifications that enter the OBERBECK-BOUSSINESQ approximation and its DSC formulation, a set of numerical results are displayed to illustrate and validate the approach.

2. Elements of DSC schemes

Given a mesh cell, a *port* is a vector valued distribution associated to a cell face which assigns a state vector $z^p = (p, Z)$ to a physical field Z (any suitable smooth vector valued function in space-time).

We also require that, within the given cell, a *nodal image* p^\sim of p exists, such that

$$(1) \quad (p^\sim, Z) = (p \circ \sigma, Z) = (p, Z \circ \sigma^{-1}),$$

for every Z (of class C^∞ , e.g.), where σ denotes the spatial translation $\sigma: \mathbb{R}^3 \rightarrow \mathbb{R}^3$ that shifts the geometrical node (centre of cell) onto the (centre of) the respective face, cf. Fig1.

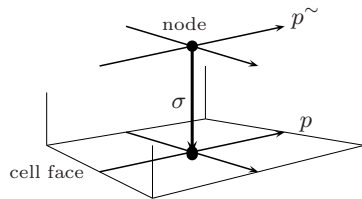


Fig. 1. Port on a cell face with nodal image.

DSC fields split thus into *port* and *node* components, z^p and z^n , which represent the field on the cell surfaces and within the cells. The two components are updated at even and odd integer multiples, respectively, of half a timestep τ and are usually constantly continued as step functions over the subsequent time intervals of length τ

Moreover, we assume that the updating instructions are *explicit*, i.e., with possibly time dependent functions F and G , for $t = m\tau$; $m \in \mathbb{N}$

$$(2) \quad \begin{aligned} z^n(t + \frac{\tau}{2}) &:= F([z^p]_t, [z^n]_{t - \frac{\tau}{2}}), \\ z^p(t + \tau) &:= G([z^p]_t, [z^n]_{t + \frac{\tau}{2}}), \end{aligned}$$

where $[z]_t$ stands for the entire sequence up to time t

$$[z]_t := (z(t - \mu\tau))_{\mu \in \mathbb{N}}$$

and we agree upon fixing $z^{p,n}(t) := 0$ for $t < 0$. (The 'back in time running' form of the sequence has certain technical advantages, cf. [He1].)

A fundamental DSC principle is *near-field interaction*, which is related to the COURANT-LEVI stability criterion in spelling that every updated state depends only on states (up to present time t) in the immediate neighbourhood. More precisely: The next nodal state depends only on states (along with their history) in the same cell and on its boundary, and a subsequent port state depends only on states (with history) on the same face and in the adjacent nodes.

As a consequence of near-field interaction, every DSC process allows for an interpretation as a multiple scattering process in the following sense.

If M is a mesh cell system and $\partial\zeta$ denotes the boundary of cell $\zeta \in M$, then every DSC state permits a unique *scattering channel representation* in the space

$$P := \prod_{\zeta \in M} \prod_{p \in \partial\zeta} (z_\zeta^p, z_\zeta^{p\sim}),$$

with canonical projections $\pi_\zeta^{p,n} : P \rightarrow P_\zeta^{p,n}$ into the port and node components of cell ζ (the cell index can usually be omitted without danger of confusion). Also, there is a natural involutory isomorphism $nb : P \rightarrow P$

$$nb : (z^p, z^{p\sim}) \mapsto (z^{p\sim}, z^p),$$

which is called the *node-boundary map* and obviously maps P^p onto P^n and vice versa. For every DSC process $z = (z^p, z^n)(t)$, the following *incident* and *outgoing fields* z_{in}^p and z_{out}^n are then recursively well defined, and are processes in P^p and P^n , respectively:

For $t < 0$, $z_{in}^p(t) := z_{out}^n(t - \frac{\tau}{2}) := 0$, and for every $0 \leq t = m\tau$; $m \in \mathbb{N}$

$$(3) \quad \begin{aligned} z_{in}^p(t) &:= z^p(t) - nb \circ z_{out}^n(t - \frac{\tau}{2}), \\ z_{out}^n(t + \frac{\tau}{2}) &:= z^n(t + \frac{\tau}{2}) - nb \circ z_{in}^p(t). \end{aligned}$$

At every instant holds, hence, $z^p(t) = nb \circ z_{out}^n(t - \frac{\tau}{2}) + z_{in}^p(t)$ and $z^n(t + \frac{\tau}{2}) = nb \circ z_{in}^p(t) + z_{out}^n(t + \frac{\tau}{2})$. Then, near-field interaction implies that every state is only a function of states incident (up to present time t) on scattering channels connected to the respective node or face.

More precisely, by induction holds

Theorem 1 . A pair of functions \mathcal{R} and \mathcal{C} exists, such that for every cell $\zeta \in M$ the process $z_\zeta^n = \pi_\zeta^n \circ z$ complies with

$$(4) \quad z_\zeta^n(t + \frac{\tau}{2}) = \mathcal{R}((z_{in}^p(t - \mu\tau))_{p \in \partial\zeta; \mu \in \mathbb{N}})$$

and the port process $z_\zeta^p = \pi_\zeta^p \circ z$ satisfies

$$(5) \quad z_\zeta^p(t + \tau) = \mathcal{C}((z_{out}^n(t + \frac{\tau}{2} - \mu\tau))_{n|\partial\zeta; \mu \in \mathbb{N}}).$$

(' | ' short-hand for 'adjacent to')

Remarks

(i) The statements immediately imply that $z_{\zeta, out}^n$ and $z_{\zeta, in}^p$ are themselves functions of states incident on connected scattering channels, since

$$(6) \quad \begin{aligned} z_{\zeta, out}^n(t + \frac{\tau}{2}) &= \mathcal{R}((z_{in}^p(t - \mu\tau))_{p \in \partial\zeta; \mu \in \mathbb{N}}) - z_{\zeta, in}^p(t) \quad \text{and} \\ z_{\zeta, in}^p(t) &= \mathcal{C}((z_{out}^n(t - \frac{\tau}{2} - \mu\tau))_{n|p; \mu \in \mathbb{N}}) - z_{\zeta, out}^{\sim p}(t - \frac{\tau}{2}) \end{aligned}$$

- (ii) \mathcal{R} and \mathcal{C} are named the *reflection* and *connection* maps, respectively, of the DSC algorithm.
- (iii) Near field interaction implies computational stability, if the reflection and connection maps are contractive or α -passive [He2], in addition.

3. The dynamic equations

The DSC algorithm is thus simply characterized as a two-step explicit scheme that alternately updates states in ports and nodes of a cellular mesh and which, in virtue of a near-field interaction principle, allows for a canonical interpretation as a scattering process, the latter exchanging *incident* and *reflected* quantities between cells and their interfaces.

Ports and nodes are related to physical fields by vector valued distributions that evaluate the fields on cell faces and within cells of a cellular mesh. Such a distribution may be a *finite integral* - as is the case with the TLM method, where finite path integrals over electric and magnetic fields are evaluated in a discrete approximation to Maxwell's integral equations [He3]. In the simplest case, it is a *Dirac measure* that pointwise evaluates a field (or a field component) within a cell and on its surface. The distribution can also be a composite of Dirac measures that evaluate a field at different points in the cell - which applies, for instance, to the gradient functional treated in sect. 4.

Classical thermodynamics with, in particular, energy conservation entail the *convection-diffusion* equation for the temperature T in a fluid of velocity \mathbf{u} with constant thermal diffusivity α , heat source(s) q , and negligible viscous heat dissipation, viz.

$$(7) \quad \frac{\partial T}{\partial t} + \mathbf{u} \cdot \text{grad } T = \alpha \Delta T + q.$$

This is the energy equation for *Boussinesq-incompressible* fluids, e.g. [GDN]. The Navier-Stokes *momentum equations* for a fluid of dynamic viscosity μ , under pressure p , and in a gravitational field of acceleration \mathbf{g} require

$$(8) \quad \frac{\partial}{\partial t}(\varrho \mathbf{u}) + (\mathbf{u} \cdot \text{grad})(\varrho \mathbf{u}) + \text{grad } p = \mu \Delta \mathbf{u} + \varrho \mathbf{g}.$$

The *Oberbeck-Boussinesq* approximation [Obb],[Bss] starts from the assumption that the fluid properties are constant, except fluid density, which only in the gravitational term varies linearly with temperature; and that viscous dissipation can be neglected. Equations (8) become so with $\varrho_\infty = \text{const}$ and $\varrho(T) = \varrho_\infty \beta(T(t, \mathbf{x}) - T_\infty)$; $\beta := \varrho^{-1} \partial \varrho / \partial T$

$$(9) \quad \frac{\partial \mathbf{u}}{\partial t} + (\mathbf{u} \cdot \text{grad}) \mathbf{u} + \frac{\text{grad} p}{\varrho_\infty} = \frac{\mu}{\varrho_\infty} \Delta \mathbf{u} + \beta(T(t, \mathbf{x}) - T_\infty) \mathbf{g}.$$

Applying the Gauss-Ostrogradski theorem to the integrals over $\Delta = \text{div grad}$ on cell ζ with boundary $\partial \zeta$ and using $\mathbf{u} \cdot \text{grad} f + f \text{div} \mathbf{u} = \text{div}(f \mathbf{u})$, equations (7, 9) yield, with a time increment τ , the following updating instructions for nodal T and \mathbf{u} , the latter, along with q , averaged over the cell volume V_ζ

$$(10) \quad T(t + \frac{\tau}{2}) := T + \tau(T \text{div} \mathbf{u} + q) + \frac{\tau}{V_\zeta} \int_{\partial \zeta} (\alpha \text{grad} T - T \mathbf{u}) \cdot dF$$

and

$$(11) \quad \mathbf{u}(t + \frac{\tau}{2}) := \mathbf{u} + \tau(\mathbf{u} \text{div} \mathbf{u} - \beta(T - T_\infty) \mathbf{g} - \frac{\text{grad} p}{\varrho_\infty}) + \frac{\tau}{V_\zeta} \left\{ \int_{\partial \zeta} \frac{\mu}{\varrho_\infty} \text{grad} \mathbf{u} \cdot dF - \int_{\partial \zeta} \mathbf{u} (\mathbf{u} \cdot dF) \right\}$$

In equations (10) and (11) the last former updates (at time $t - \tau/2$) of the nodal quantities enter the right-hand sides in the first line, and the former updates (at time t) of the cell face quantities enter the second line. Note that $\text{div} \mathbf{u}$ vanishes, of course, for incompressible flow.

All nodal values of T and \mathbf{u} are thus updated at the reflection step of the algorithm, while the cell face quantities that enter the integrals at the right-hand sides are updated on the connection step. In next section we will see how to proceed with an unstructured (non-orthogonal) hexahedral mesh.

4. Non-orthogonal hexahedral cell

The physical interpretation of a DSC algorithm associates a smoothly varying (e.g. in time and space C^∞ -) scalar or vector field Z to port and node states z^p and z^n of a mesh cell system.

Let any hexahedral cell be given by its eight vertices. Define then *edge vectors* $(\nu e)_{\nu=0, \dots, 11}$, *node vectors* $(\mu b)_{\mu=0, 1, 2}$, and *face vectors* $(\iota f)_{\iota=0, \dots, 5}$, using the labelling scheme of figure 2 a

$$(12) \quad \begin{aligned} \mu b &:= \frac{1}{4} \sum_{\nu=0}^3 ({}_{4\mu+\nu} e) & \mu &= 0, 1, 2 \\ \text{and } \iota f &:= \frac{(-1)^\iota}{4} (({}_{8+2\iota} e + ({}_{9+2(\iota+(-1)^\iota)} e) \wedge \\ & \quad \wedge ({}_{4+2\iota} e + ({}_{5+2\iota} e) & \iota &= 0, \dots, 5, \end{aligned}$$

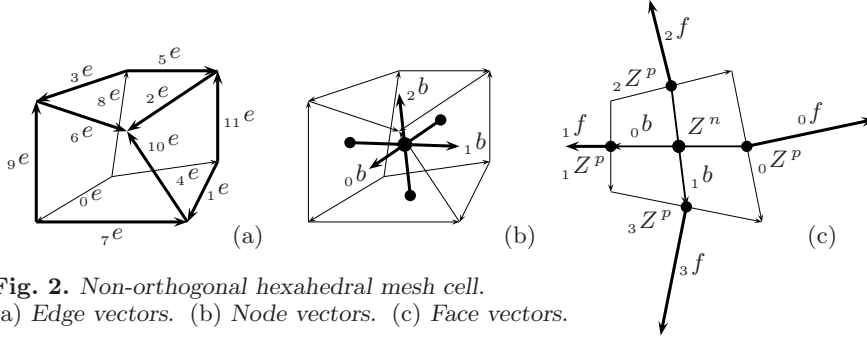


Fig. 2. Non-orthogonal hexahedral mesh cell.
(a) Edge vectors. (b) Node vectors. (c) Face vectors.

with all indices understood cyclic modulo 12 and \wedge denoting the cross product in \mathbb{R}^3 . At every cell face $\iota \in \{0, \dots, 5\}$ and for any given $\tau \in \mathbb{R}_+$ the following time shifted finite differences of Z in directions ${}_\mu b$ ($\mu = 0, 1, 2$) form a vector valued function

$$(13) \quad {}_\iota \nabla^B Z_\mu(t) := \begin{cases} 2(-1)^\iota (Z^n|_{t-\tau/2} - {}_\iota Z^p|_t) & \text{if } \mu = \lfloor \iota/2 \rfloor \\ ({}_{2\mu+1} Z^p - {}_{2\mu} Z^p)|_{t-\tau} & \text{if } \mu \neq \lfloor \iota/2 \rfloor \end{cases}$$

($\lfloor x \rfloor$ denotes the *integer part* of $x \in \mathbb{R}$). The time increments are chosen conform with the updating conventions of DSC schemes (as will be seen in a moment) and are consistent. In fact, in the first order of the time increment τ and of the linear cell extension, the vector ${}_\iota \nabla^B Z$ in the centre point of face ι approximates the scalar products of the node vectors with the gradient ∇Z . Let, precisely, for a fixed centre point on face ι and $\epsilon \in \mathbb{R}_+$ the ϵ -scaled cell have edge vectors ${}_\iota e^\sim := \epsilon {}_\iota e$. Let also ${}_\iota \nabla^{B^\sim} Z_\mu$ denote function (13) for the ϵ -scaled cell (with node vectors ${}_\mu b^\sim = \epsilon {}_\mu b$). Then at the fixed point holds

$$(14) \quad \langle {}_\mu b, \text{grad}(Z) \rangle = {}_\mu b \cdot \nabla Z = \lim_{\epsilon \rightarrow 0} \lim_{\tau \rightarrow 0} \frac{1}{\epsilon} {}_\iota \nabla^{B^\sim} Z_\mu,$$

as immediately follows from the required C^1 -smoothness of the field Z .

To recover the gradient ∇Z from (13) in the same order of approximation, observe that for every orthonormal basis $({}_\nu u)_{\nu=0, \dots, m-1}$ of \mathbb{R}^m or \mathbb{C}^m , and for any basis $({}_\mu b)_{\mu=0, \dots, m-1}$ with coordinate matrix $\beta_\nu^\mu = \langle {}_\nu u, {}_\mu b \rangle$, the scalar products of every vector a with ${}_\mu b$ equal

$$(15) \quad \underbrace{\langle {}_\mu b, a \rangle}_{=: \alpha_\mu^B} = \sum_{\nu=0}^{m-1} \underbrace{\langle {}_\mu b, {}_\nu u \rangle}_{(\bar{\beta}_\mu^\nu = (\beta_\nu^\mu)^*)} \underbrace{\langle {}_\nu u, a \rangle}_{=: \alpha_\nu} = \bar{\beta}_\mu^\nu \alpha_\nu$$

(at the right-hand side, and henceforth, we observe EINSTEIN's summation convention - without yet summing up over indices that anywhere appear as left-hand subscripts), hence

$$(16) \quad \alpha_\nu = \gamma_\nu^\mu \alpha_\mu^B, \quad \text{with} \quad (\gamma_\nu^\mu) := ((\beta_\nu^\mu)^*)^{-1}.$$

I.e., the scalar products of any vector with the basis vectors ${}_\mu b$ transform into the coordinates of that vector with respect to an orthonormal basis ${}_\nu u$

by multiplication with matrix $\gamma = (\beta^*)^{-1}$, where $\beta_\nu^\mu = \langle \nu u, \mu b \rangle$, i.e. β is the matrix of the coordinate (column) vectors μb with respect to the given ON-basis νu , and γ its adjoint inverse.

This applied to the node vector basis μb and (14) yields the approximate gradient of Z at face ι

$$(17) \quad \iota \nabla Z_\nu = \gamma_\nu^\mu \iota \nabla^B Z_\mu.$$

The scalar product of the gradient with face vector $\iota f^\nu = \langle \iota f, \nu u \rangle$, $\nu \in \{0, 1, 2\}$ is thus

$$(18) \quad \iota S = \iota f \cdot \iota \nabla Z = \underbrace{\iota f^\nu \gamma_\nu^\mu}_{=: \iota s^\mu} \iota \nabla^B Z_\mu = \iota s^\mu \iota \nabla^B Z_\mu.$$

Continuity of the gradient at cell interfaces yields linear updating equations for Z^p on the two adjacent faces. In fact, for any two neighbouring cells ζ , χ with common face, labelled ι in cell ζ and κ in χ , continuity requires

$$(19) \quad \zeta S = -\kappa S.$$

Substituting (18) for ζS and κS and observing the time shifts in (13) provides the updating relations for Z^p at the cell interfaces. To make these explicit, we first introduce the quantities $\iota z_\mu^{p,n}$, ($\iota = 0, \dots, 5$; $\mu = 0, 1, 2$)

$$(20) \quad \iota z_\mu^n(t) := \begin{cases} 2(-1)^\iota Z^n|_t & \text{if } \mu = [\iota/2] \\ (2_{\mu+1} Z^p - 2_\mu Z^p)|_{t-\tau/2} & \text{else} \end{cases},$$

which in virtue of (1) yields $\iota z_\mu^p = (p, Z) = (p^\sim, Z \circ \iota \sigma^{-1}) = \iota z_\mu^n | Z \circ \iota \sigma^{-1}$, where $\iota \sigma : n \mapsto p$ denotes the nodal shift pertinent to face ι . In particular

$$(21) \quad \iota z_{[\iota/2]}^p(t) = 2(-1)^\iota \iota Z^p|_t,$$

which together with (20) is consistent for $\mu \neq [\iota/2]$ with

$$(22) \quad \iota z_\mu^n(t + \tau/2) = -\frac{1}{2} (2_{\mu+1} z_\mu^p + 2_\mu z_\mu^p)(t).$$

From (13, 18, 20, 21) follows that

$$(23) \quad \begin{aligned} \iota S|_{t+\tau} &= \iota s^\mu (\iota z_\mu^n|_{t+\tau/2} - 2(-1)^\iota \delta_\mu^{[\iota/2]} \iota Z^p|_{t+\tau}) \\ &= \iota s^\mu (\iota z_\mu^n|_{t+\tau/2} - \delta_\mu^{[\iota/2]} \iota z_\mu^p|_{t+\tau}). \end{aligned}$$

The continuity of Z , i.e. $\zeta Z^p = \kappa Z^p$, the implies with (19,20)

$$(24) \quad \zeta z_{[\iota/2]}^p(t + \tau) = \frac{\zeta s^\mu \zeta z_\mu^n(t + \tau/2) + \kappa s^\nu \kappa z_\nu^n(t + \tau/2)}{\zeta s^{[\iota/2]} + (-1)^{\iota+\kappa} \kappa s^{[\kappa/2]}}.$$

For completeness we agree upon setting $\zeta z_\mu^p(t + \tau) := \zeta z_\mu^n(t + \tau/2)$ for $\mu \neq [\iota/2]$ (which yet contains a slight inconsistency, in that continuity might be infringed; this can be remedied by taking the arithmetic means of

the two adjacent values). - In fact, our agreement doesn't do harm, since any discontinuity disappears with mesh refinement.

We have, hence, a complete set of recurrence relations for z^p (given z^n by the former reflection step) which at the same time determine the field components on face ι and their gradients

$$(25) \quad \iota \nabla Z_\nu = \gamma_\nu^\mu \iota z_\mu^p.$$

Essentially this constitutes the connection step of the algorithm.

Nodal gradients are similarly (yet even more simply) derived using

$$\nabla^B Z_\mu^n \left(t + \frac{\tau}{2} \right) := ({}_{2\mu+1}Z^p - {}_{2\mu}Z^p)(t); \quad \mu = 0, 1, 2$$

in the place of (13) and then again (17). With the node and cell-boundary values and gradients of T and \mathbf{u} the nodal updating relations for the latter are immediately extracted from equations (10, 11) in sect. 3. For equation (10) this is essentially (up to the convective term) carried out in [He1], sect. 5, and the procedure remains straightforward in the case at hand. Note that a well-timed LES coarsening routine [He3] should be periodically carried out before the nodal step of iteration in order to avoid instabilities from the energy cascade [Po].

The updating relations thus obtained are explicit and consistent with near-field interaction (only adjacent quantities enter). So, they can optionally be transformed into scattering relations for incident and reflected quantities (3) along the guidelines of section 2 - with established advantages for stability estimates [He2].

5. Pressure

Conservation of mass simply requires divergence-free flow, $div \mathbf{u} = 0$, for a Boussinesq-incompressible fluid. In integral form, using Gauss' Theorem, this means $0 = \int_\zeta div \mathbf{u} dV = \int_{\partial\zeta} \mathbf{u} \cdot dF$. Since equations (7, 8) in section 3 do not a priori guarantee this, additional arrangements must be made. This is done by the following procedure, which in Magneto-Hydrodynamics is known as *divergence cleaning*.

In a successive overrelaxation (SOR) routine, carried out between the connection and reflection steps of the iteration cycle, firstly the (discrete) cell boundary integrals $I_{\partial\zeta} = \int_{\partial\zeta} \mathbf{u} \cdot dF$ are computed and then the pressure p which compensates $I_{\partial\zeta}$ so that

$$(26) \quad \frac{\tau}{\varrho_\infty} \int_{\partial\zeta} grad p \cdot dF = \int_{\partial\zeta} \mathbf{u} \cdot dF.$$

Taking indeed Z of the preceding section as the pressure, equations (26) (of course, in discrete form with sums over the cell faces) yield a unique solution $p^n = Z^n$ for every cell, given the right-hand side integral $I_{\partial\zeta}$. Note that we are actually solving Poisson's equation $\Delta p = (\varrho_\infty/\tau) div \mathbf{u}$ in integral form.

With the new face pressure gradient computed in following the lines of section 4 the face values of \mathbf{u} are updated as $\mathbf{u} - (\tau/\varrho_\infty) grad p$.

After each SOR cycle, continuity of $grad p$ at the cell faces is restored by updating the port values of p according to the instructions of the last section. The loop of processes is reiterated until $\sum_{\zeta} I_{\partial\zeta} < \epsilon$ for a suitable bound ϵ (which happens after a few iterations for appropriate choices).

6. Convection in coaxial line

We illustrate the approach in a stalwart application by displaying the results of simulations with coaxial line RL100-230 under high power operating conditions (which are realistically inferred from a ion cyclotron resonance heating *ICRH* experiment in plasma physics).

The inner and outer conductors of diameters 100 mm and 230 mm are made of copper and aluminium, respectively, and the rigid line is filled with air at atmospheric pressure. The heating process has been simulated from standby to steady state CW operation, at frequency 100 MHz and 160 kW transmitted power, for horizontal position of the line and with outer conductor cooled at 40 degrees Celsius.

Figure 3 b displays the computed air flow profile (vertical section) in steady state, which is attained some minutes after power-on. Visibly, the natural convection pattern is nicely developed.

Our computations have been carried out with a 3D-mesh of 10 layers in axial direction, over 200 millimeters of line, the transverse cross section of which is displayed in figure 3 a. At the metallic interfaces no-slip boundary conditions are implemented and free-slip conditions at all other boundaries.

Simultaneously, and using the same mesh cell system, a Maxwell field TLM algorithm was run to provide the heat sources.

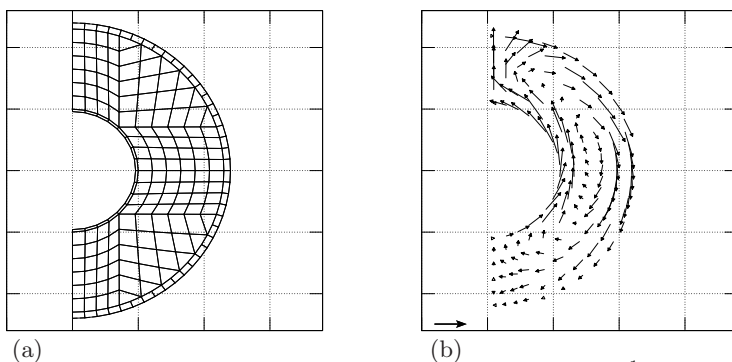


Fig. 3. (a) mesh (b) velocity profile [reference arrow: 0.1 ms^{-1}]

7. Conclusion

A prototypical implementation of the OBERBECK-BOUSSINESQ approximation to viscous flow has been presented in this paper, which demonstrates

the fundamental fitness of the DSC approach for fluid dynamic computations. DSC schemes thus significantly transcend the range of application of the TLM method from which they descend.

A next natural step in the line of this study is the implementation of turbulence models which are compatible with the BOUSSINESQ approach, such as the $k - \epsilon$ model [ATP], first of all. Another objective is the incorporation of compressible flow.

- We hope this paper stimulates some interest into joint further investigation in these directions.

References

- [MeSt] Meister, A., Struckmeier, J., *Hyperbolic Partial Differential Equations* Theory, Numerics and Applications, Friedrich Vieweg and Sohn, Göttingen 2002
- [LeVeque] LeVeque, R.J., Mihalas, D., Dorfi, E.A., Müller, E. *Computational Methods for Astrophysical Fluid Flow*, Saas Fee Advanced Courses, 27, Springer-Verlag Berlin Heidelberg, 1998
- [GDN] Griebel, M., Dornseifer, T., Neunhoffer, T., *Numerical Simulation in Fluid Dynamics*, SIAM monographs on mathematical modeling and computation, Society for Industrial and Applied Mathematics, 1998
- [Po] Pope, S.B., *Turbulent flows*, Cambridge University Press, Cambridge 2000.
- [ATP] Anderson, D.A., Tannehill, J.C., Pletcher, R.H., *Computational Fluid Mechanics and Heat Transfer*, series in computational methods in mechanics and thermal sciences, Hemisphere Publishing Corporation, 1984
- [Bss] Boussinesq, J., *Théorie Analytique de la Chaleur*, Gauthiers-Villars, 2., Paris 1903
- [Obb] Oberbeck, A., Über die Wärmeleitung der Flüssigkeiten bei Berücksichtigung der Strömung infolge Temperaturdifferenzen., Ann. Phys. Chem., vol. 7, pp. 271-292, 1879
- [JoB] Johns, P.B., Beurle R.L., Numerical solution of 2-dimensional scattering problems using transmission line matrix, Proc. IEEE, vol. 118, pp. 1203-1208, 1971
- [He0] Hein, S., Finite-difference time-domain approximation of Maxwell's equations with nonorthogonal condensed TLM mesh, Int. J. Num. Modelling, vol. 7, pp. 179-188, 1994
- [He1] Hein, S., Dual scattering channel schemes extending the JOHNS Algorithm <http://arxiv.org/abs/math.NA/0309261>, March 2004
- [He2] Hein, S., On the stability of dual scattering channel schemes, <http://arxiv.org/abs/math.NA/0405095>, May 2004
- [He3] Hein, S., Large eddy approximation of turbulent flow in DSC schemes, <http://arxiv.org/abs/math.NA/0603704>, March 2006
- [He4] Hein, S., TLM numerical solution of Bloch's equations for magnetized gyrotropic media, Appl. Math. Modelling, vol. 21, pp. 221-229, 1997